Response to Reviewer 1 Comments

We truly grateful for the reviewers for the valuable and constructive comments, which are very useful for the improvement of the manuscript. We have revised the manuscript carefully according to the reviewers' comments. Point–to–point responses are given below. The original comments are black in color, while our responses are in blue. The revised parts in the manuscript are marked in red. All the page number and line number are referred to the revised manuscript.

General comments:

Point 1: It's hard for me to identify the main topic of this paper. While the primary focus appears to be explaining the opposing trends in the 98th and 2nd percentiles of ozone in the MLYRP (part of eastern China), the paper includes many other analyses that are irrelevant to this topic. For instance, Section 3.4 (Interannual differences in surface O_3 formation sensitivity) and Section 3.6 (Key meteorological and anthropogenic factors inducing O_3 pollution) should be removed (they haven't found anything new in these sections either). The entire paper should be reframed. Additionally, Section 3.5 presents the same analysis and draws the same conclusions as Sections 3.1–3.3 but for a larger area (eastern China). The inclusion of Section 3.5 seems redundant. Why don't the authors focus on eastern China throughout the manuscript?

Response 1: We apologize for the confusion generated by the previous version of the manuscript and sincerely hope that our logic is now easier to follow with this new version. We have followed the reviewer's comments and reorganized the manuscript to avoid diverting the reader's attention. Firstly, we have deleted sections 3.4 (Interannual differences in surface O_3 formation sensitivity) and 3.6 (Key meteorological and anthropogenic factors inducing O_3 pollution) in the previous manuscript. Then, sections 3.1–3.3 and 3.5 was reframed, and the entire updated manuscript focuses on eastern China throughout the manuscript.

The new manuscript mainly includes four parts. First, we report long–term records of surface O_3 and related parameters observed at urban air quality monitoring sites and by satellites in eastern China, characterizing the trends of low, typical, and peak surface O_3 concentrations during the warm season (May–September) from 2017 to 2022. Then, a Multiple Linear Regression (MLR) model is used to evaluate the anthropogenic and meteorological contributions to the 98th and 2nd O_3 percentile trends. Next, secondary formaldehyde (HCHO) and NO_2 are employed to diagnose the diurnal variations in O_3 formation sensitivity and investigate the reasons for peak O_3 concentration trends in the context of current NO_x reduction.

Finally, we discuss the reasons for the potential increase in low O_3 concentrations and the sensitivity of peak and low O_3 trends during the study period. Please refer to our new manuscript for details.

In addition, following the referee's suggestion, the manuscript was edited by Elsevier Language Editing Services (please see the following Elsevier certificate).

Fig. R1 Certificate of Elsevier language editing services

Point 2: To understand the drivers of ozone trends, the authors use Multiple Linear Regression (MLR) to separate meteorological influences. There are several issues with their analysis: (a) The predicted variable, O_3 concentration, should also be normalized in the MLR. Normalizing Y first would eliminate the need for natural background O_3 in equation (2). (b) Line 27, Page 6, the statement that O_3 from natural sources is stable is incorrect. Biogenic VOCs and soil NOx emissions are highly sensitive to temperature. (c) Lines 19–21, 23–24, Page 10, the authors seem to confuse the terms "interannual fluctuation" and "trend." The trend observed is actually a low–frequency signal after removing the high–frequency signals (interannual fluctuation). In this part, it is only acceptable to conclude that the anthropogenic component drives the trend, but it is apparent that meteorological parameters dominate the interannual fluctuation (as it roughly reproduces the peaks and troughs). All of this needs to be corrected.

Response 2: We thank the reviewer for pointing out this issue. (a) We corrected the problem (the predicted variable, O_3 concentration, should also be normalized in the MLR. Normalizing Y first would eliminate the need for natural background O_3 in equation 2) in the MLR model, and rearranged this subsection to conclude that, although anthropogenic emissions are the main driver of the opposing trends in peak and low O_3 concentrations in eastern China, the effect of

the change of meteorological component on 2nd or 98th O_3 percentiles trends cannot be ignored. (b) The statements in Line 27, Page 6 have been deleted, and (c) Lines 19–21, 23–24, Page 10 have been corrected.

In the new manuscript, we used the same stepwise MLR modeling approach as (Zhai et al., 2019; Li et al., 2018; Li et al., 2020; Liu et al., 2023). Following Liu et al. (2023) and Li et al. (2020), the MLR model fitted the deseasonalized and detrended 10 d mean 98th or 2nd O_3 percentile time series to the deseasonalized and detrended 10 d mean meteorological variables. The deseasonalized and detrended time series data were constructed by removing the 50 d moving average data from the 10 d moving average data. The stepwise MLR model has the following form:

$$Y(t) = R + \sum_{k=1}^{n} \beta_k X_k(t) \tag{1}$$

Where $Y(t)$ is the deseasonalized and detrended daily surface 98th or 2nd O_3 percentile time series, R is the regression constant, β_k is the regression coefficient, and X_k is the deseasonalized and detrended daily meteorological variable considered as a possible O_3 covariate. Stepwise regressions were performed, adding and removing terms based on their independent statistical significance to obtain the best model fit.

Daily meteorological variables were obtained from the ERA5 reanalysis data (Download from https://cds.climate.copernicus.eu, last access: January 7, 2024), included temperature (T, °C), surface relative humidity (RH, %), total cloud cover (TCC), total precipitation (TP, mm), mean sea level pressure (MSLP, hPa), wind speed of U, V components (U, V, m/s), boundary layer height (BLH, m), and vertical velocity at 850 hPa (V850, m/s).

First, we used the MLR model to remove the effects of meteorological variability from the 2017 to 2022 98th or 2nd O_3 percentile trends. We apply Eq. (1) to the meteorological anomalies X_k during May–September 2017–2022, obtained by removing the 6–year means of the 50 d moving averages from the 10 d mean time series. The anomalies calculated in this process were deseasonalized but not detrended. This yields the meteorology–driven 98th or 2nd O_3 percentile anomalies $Y_m(t)$

$$Y_m(t) = R + \sum_{k=1}^{n} \beta_k X_k(t) \tag{2}$$

Secondly, to avoid overfitting, only the three most important meteorological parameters were selected based on their individual contributions to the regressed 98th or 2nd O_3 percentiles, along with the requirement that they be statistically significant above the 95% confidence level

in the MLR model (Li et al., 2018). The fit results and selected meteorological variables varied by city but were regionally consistent (Table R1 and Table R2). The 98th or 2nd O_3 percentile anomalies $Y_a(t)$ obtained by deseasonalizing, but not detrending, the 98th or 2nd O_3 percentile time series in a similar manner as for the meteorological variables (by removing the 6–year means of the 50 d moving averages). The residual anomaly $Y_r(t)$ after removing the meteorology–driven 98th or 2nd O_3 percentile anomalies from the MLR model is given by

$$Y_r(t) = Y_a(t) - Y_m(t) \tag{3}$$

Finally, the residual is an anomalous component that cannot be explained by the MLR meteorological model and is referred to as meteorologically corrected data by (Zhai et al., 2019). It consists of noise due to the limitations of the MLR model and other factors and can be mainly attributed to long–term trends in anthropogenic emission changes over a 6–year period. The trend in the regressed 98th or 2nd O_3 percentile reflected the meteorological contribution, and the residual was then used to reflect the presumed anthropogenic contribution. For the updated MLR model, please refer to section 2.4 in the manuscript.

Table R1. Meteorological drivers of 2% O_3 percentile and Pearson correlation coefficient between observed and modeled 2% O_3 percentile in each city of eastern China during May–September 2017–2022

| | Meteorological variable | | | | | Meteorological variable | | | |
	1st	2st	3st	R		1st	2st	3st	R
Taian	T	RH	U	0.35	Beijing	U	RH	T	0.23
Puyang	T	BLH	RH	0.50	Tianjing	U	T	RH	0.32
Rizhao	U	V	T	0.46	Baoding	U	RH	TP	0.27
Jining	RH	T	V	0.54	Lanfang	U	T	V	0.23
Xinxiang	U	RH	V	0.41	Shijiazhuang	RH	BLH	U	0.27
Jiaozuo	T	RH	U	0.39	Handan	RH	V	BLH	0.20
Heze	RH	T	V	0.47	Qinghuangdao	V	U	RH	0.32
Linyi	RH	U	TP	0.40	Cangzhou	BLH	T	MSLP	0.28
Kaifeng	RH	U	T	0.49	Xingtai	RH	BLH	U	0.17
Zhengzhou	BLH	RH	U	0.47	Hengshui	T	V	RH	0.28
Luoyang	BLH	RH	V	0.16	Tangshan	U	V	RH	0.20
Zaozhuang	RH	T	U	0.46	Jinan	V	BLH	RH	0.59
Lianyungang	RH	V850	U	0.37	Qingdao	V	BLH	RH	0.26
Shangqiu	RH	T	V	0.48	Zibo	V	BLH	RH	0.59
Xuzhou	RH	BLH	V	0.48	Dongying	U	V	V850	0.36
Xuchang	BLH	RH	U	0.53	Yantai	V	BLH	U	0.33
Suqian	RH	T	MSLP	0.40	Weifang	BLH	T	U	0.34
Huaibei	RH	U	BLH	0.59	Weihai	RH	U	MSLP	0.36
Pingdingshan	BLH	RH	U	0.57	Dezhou	RH	V	BLH	0.40
Bozhou	RH	V	T	0.49	Liaocheng	BLH	V	RH	0.48
Zhoukou	RH	U	T	0.49	Binzhou	BLH	T	V	0.23
Luohe	RH	U	MSLP	0.45	Shaoxing	RH	BLH	T	0.59
Suzhou	RH	U	BLH	0.50	Jinhua	RH	TP	V	0.60
Huaian	RH	V	TP	0.42	Taizhou	V	RH	U	0.54
Yancheng	V	RH	BLH	0.37	Ningbo	RH	V	TP	0.48

Nanyang	RH	U	BLH	0.67	Wuhan	RH	V	BLH	0.61
Zhumadian	RH	TP	BLH	0.52	Changsha	RH	V	BLH	0.71
Fuyang	RH	V	U	0.64	Jinghzou	RH	V	BLH	0.55
Bengbu	RH	BLH	U	0.36	Yueyang	RH	BLH	V	0.60
Huainan	RH	BLH	U	0.56	Zhuzhou	RH	V	BLH	0.73
Xinyang	RH	TP	T	0.63	Xiangtan	RH	V	BLH	0.72
Suizhou	RH	BLH	U	0.63	Yichang	RH	U	V850	0.64
Shanghai	RH	V	TP	0.55	Yiyang	RH	V	BLH	0.67
Nanjing	V	RH	T	0.40	Changde	V	BLH	RH	0.59
Wuxi	RH	V	BLH	0.57	Jingmen	V	RH	U	0.63
Changzhou	V	RH	TP	0.49	Huangshi	RH	U	V850	0.72
Suzhou	RH	V	T	0.52	Huanggang	RH	U	V850	0.77
Nantong	V	RH	U	0.62	Xianning	RH	U	MSLP	0.74
Yangzhou	V	RH	T	0.52	Xiaogan	RH	V850	BLH	0.68
Zhenjiang	V	RH	T	0.55	Quzhou	V	RH	U	0.68
Taizhou	V	RH	T	0.59	Lishui	RH	V	T	0.70
Luan	RH	V	T	0.24	Wenzhou	RH	V	U	0.63
Hangzhou	RH	V	BLH	0.53	Jiujiang	V	RH	MSLP	0.58
Jiaxing	RH	V	T	0.45	Nanchang	V	RH	V850	0.67
Huzhou	V	RH	U	0.61	Jingdezhen	BLH	V850	T	0.59
Hefei	RH	TP	V	0.37	Shangrao	V850	BLH	RH	0.65
Wuhu	V	TP	U	0.46	Yingtan	BLH	V850	RH	0.64
Maanshan	V	U	TP	0.45	Yichun	V850	U	T	0.63
Tonglin	V	T	TP	0.50	Fuzhou	RH	V	BLH	0.72
Anqing	V	T	TP	0.56	Jian	BLH	U	RH	0.57
Chuzhou	RH	V	BLH	0.44	Xinyu	BLH	V	U	0.62
Chizhou	RH	V	BLH	0.47	Pingxiang	V850	BLH	T	0.61
Xuancheng	T	RH	U	0.27	-	-	-	-	-

Table R2. Meteorological drivers of 98% O_3 percentile and Pearson correlation coefficient between observed and modeled 98% O_3 percentile in each city of eastern China during May–September 2017–2022

	Meteorological variable					Meteorological variable			
	1st	2st	3st	R		1st	2st	3st	R
Taian	T	TP	TCC	0.71	Beijing	MSLP	BLH	V	0.30
Puyang	T	V850	TP	0.79	Tianjing	V	MSLP	BLH	0.27
Rizhao	T	U	TCC	0.67	Baoding	MSLP	V	BLH	0.28
Jining	T	TP	V850	0.77	Lanfang	MSLP	BLH	V	0.32
Xinxiang	T	TCC	BLH	0.74	Shijiazhuang	MSLP	BLH	V	0.24
Jiaozuo	T	TP	TCC	0.81	Handan	T	MSLP	U	0.31
Heze	T	V850	TP	0.78	Qinghuangdao	TCC	U	MSLP	0.36
Linyi	T	TP	TCC	0.73	Cangzhou	V	BLH	MSLP	0.35
Kaifeng	T	V850	TP	0.78	Xingtai	MSLP	BLH	V	0.25
Zhengzhou	T	V850	TP	0.78	Hengshui	V	MSLP	BLH	0.38
Luoyang	U	TCC	V	0.28	Tangshan	TCC	MSLP	T	0.27
Zaozhuang	T	TP	TCC	0.81	Jinan	T	TP	V850	0.77
Lianyungang	TCC	U	TP	0.68	Qingdao	U	BLH	RH	0.45
Shangqiu	T	TP	V850	0.71	Zibo	T	TP	V850	0.70
Xuzhou	T	TCC	TP	0.74	Dongying	T	RH	V	0.66
Xuchang	T	V850	TCC	0.70	Yantai	U	T	RH	0.44
Suqian	RH	TCC	TP	0.74	Weifang	T	TP	U	0.68
Huaibei	TCC	T	TP	0.74	Weihai	U	T	RH	0.44
Pingdingshan	T	V850	U	0.66	Dezhou	T	TP	V850	0.75
Bozhou	TCC	T	TP	0.67	Liaocheng	T	V850	TP	0.77
Zhoukou	T	TCC	RH	0.73	Binzhou	T	TP	V	0.66
Luohe	T	V850	RH	0.75	Shaoxing	T	V	TP	0.66

Suzhou	TCC	T	TP	0.71	Jinhua	T	V	TP	0.59
Huaian	T	TCC	TP	0.72	Taizhou	U	V	T	0.62
Yancheng	TP	V850	U	0.56	Ningbo	T	V	U	0.69
Nanyang	T	TCC	RH	0.74	Wuhan	TCC	RH	V850	0.75
Zhumadian	TCC	BLH	TP	0.67	Changsha	RH	TCC	V	0.76
Fuyang	RH	TCC	MSLP	0.74	Jinghzou	RH	V850	T	0.84
Bengbu	T	TCC	TP	0.72	Yueyang	RH	TCC	U	0.82
Huainan	TCC	RH	MSLP	0.68	Zhuzhou	RH	V	T	0.73
Xinyang	RH	TCC	U	0.74	Xiangtan	RH	V	TCC	0.78
Suizhou	RH	TCC	MSLP	0.75	Yichang	RH	TCC	V850	0.79
Shanghai	T	U	RH	0.72	Yiyang	RH	TCC	V850	0.80
Nanjing	TCC	V850	V	0.61	Changde	TCC	V850	T	0.74
Wuxi	TP	TCC	U	0.66	Jingmen	RH	V850	T	0.76
Changzhou	TCC	TP	BLH	0.60	Huangshi	RH	TCC	V	0.76
Suzhou	T	TP	U	0.63	Huanggang	TCC	RH	U	0.72
Nantong	T	RH	BLH	0.75	Xianning	RH	V850	T	0.80
Yangzhou	TCC	TP	V850	0.61	Xiaogan	RH	TCC	U	0.72
Zhenjiang	TCC	TP	MSLP	0.61	Quzhou	RH	V850	T	0.74
Taizhou	TCC	V850	U	0.61	Lishui	RH	U	V	0.65
Luan	TCC	MSLP	T	0.61	Wenzhou	U	RH	V	0.65
Hangzhou	TP	TCC	T	0.69	Jiujiang	TCC	V850	RH	0.80
Jiaxing	T	TP	U	0.70	Nanchang	RH	V850	T	0.72
Huzhou	TP	TCC	T	0.67	Jingdezhen	RH	V850	TCC	0.75
Hefei	TCC	TP	V	0.59	Shangrao	TCC	V850	T	0.76
Wuhu	TCC	TP	V	0.65	Yingtan	TCC	V850	T	0.78
Maanshan	TCC	TP	MSLP	0.66	Yichun	V850	TCC	T	0.75
Tonglin	TCC	MSLP	V	0.63	Fuzhou	V850	T	TCC	0.82
Anqing	TCC	V	TP	0.58	Jian	TCC	T	V	0.66
Chuzhou	TCC	TP	MSLP	0.58	Xinyu	V850	TCC	V	0.75
Chizhou	TCC	V	MSLP	0.63	Pingxiang	V850	TCC	V	0.75
Xuancheng	TCC	V	MSLP	0.58	-	-	-	-	-

Point 3: The authors conclude that the continuous NO_x reduction during 2017–2022 is the reason for the differences in tendencies in the O_3 98th and 2nd percentile trends. However, if you look carefully at Figure 5, which presents the anthropogenic impact for each year on the 98th and 2nd percentile trends, respectively, you will find that the anthropogenic impact shows a similar pattern for both trends until mid–2021. It appears that something that occurred after 2021 is the main reason for the divergence. More investigation is clearly needed. Also, how is this opposing trend sensitive to the period studied?

Response 3: Thanks for your constructive comments! We have corrected the problem in the MLR model according to Point 2, and the updated results is shown in Fig.R2. The trends for the monthly mean observed, meteorological, and anthropogenic 98th O_3 percentiles concentrations during May–September 2017–2021 are -0.363 ppb/year, -0.119 ppb/year (-33%), and -0.244 ppb/year (-67%), respectively (Table R3), and the trends for the monthly mean observed, meteorological, and anthropogenic 2nd O_3 percentiles concentrations are 0.027 ppb/year, -0.044 ppb/year (-163%), 0.071 ppb/year (263%), respectively. However, the trends

of monthly mean observed, meteorological and anthropogenic of 98th O_3 percentiles during May–September 2017–2022 are -0.178 ppb/year, 0.005 ppb/year (3%) and -0.183 ppb/year (-103%), respectively, and the trends of the observed, meteorological and anthropogenic of 2nd O_3 percentiles during May–September 2017–2022 are 0.115 ppb/year, 0.008 ppb/year (7%) and 0.107 ppb/year (93%), respectively.

Although anthropogenic emissions dominated variations in O_3 trends (May–September 2017–2022 and May–September 2017–2021), meteorological effects on O_3 trends cannot be ignored, particularly in 2022. Shadowed by mid–latitude atmospheric circulation, tropical sea–air coupling, and local land–air feedback processes, a record–breaking super–heatwave event occurred in most cities in eastern China in the summer of 2022, and some cities broke their highest temperature records (Zhang et al., 2023; Zhang et al., 2022). The most important meteorological variables in the MLR model were daily maximum temperature and RH (Tables R1 and R2). The temperature in eastern China showed that the monthly mean nighttime (daytime) temperature in June–August 2022 was 1.0 °C (1.1 °C), 0.8 °C (1.4 °C) and 2.2 °C (2.8 °C) higher than the monthly mean nighttime (daytime) temperature in June–August 2021, respectively (Fig. R3). The monthly mean nighttime (daytime) RH in eastern China in 2022 was 3.2% (3.1%), 1.9% (4.5%), and 9.4% (11%) lower than the monthly mean nighttime (daytime) RH in June–August 2021, respectively. Li et al. (2024) revealed that a sustained heatwave of extremely hot and dry summers in 2022 accelerate photochemical O_3 production by increasing anthropogenic and biogenic emissions and exacerbate O_3 accumulation by inhibiting dry deposition due to water–starved vegetation, resulting in an increase in O_3 pollution by more than 30% in urban areas. Our results also showed an increase in the meteorological components in the 98th and 2nd O_3 percentiles in 2022 relative to the meteorological components in the 98th and 2nd O_3 percentiles in 2021 (Fig.R2). Therefore, extremely hot and dry weather in 2022 will increase the peak and low O_3 concentrations in eastern China, which is probably the main reason for the difference between the May and September 2017–2021 and May–September 2017–2022 meteorological component trends. The above discussion was added to the manuscript, please refer to Page 13 Line 28–32 and Page 14 Line 1–19 in the manuscript.

In addition, the high relative humidity in 2020 and 2021, as well as the impact of COVID–19 pandemic also had a significant impact on the peak and low O_3 trend, which is analyzed in detail in **Point 4**.
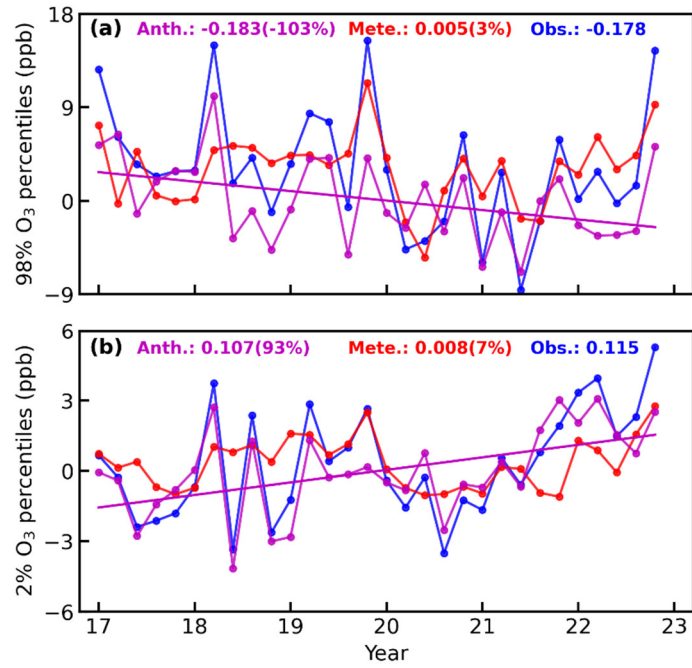
Fig.R2 Trends of observed (blue lines), meteorological (red lines), and anthropogenic (red lines) (a) 98th and (b) 2nd O₃ percentiles component in eastern China during May–September 2017–2022. The labels at the top of each panel represent the trend in observed, meteorological, and anthropogenic components.
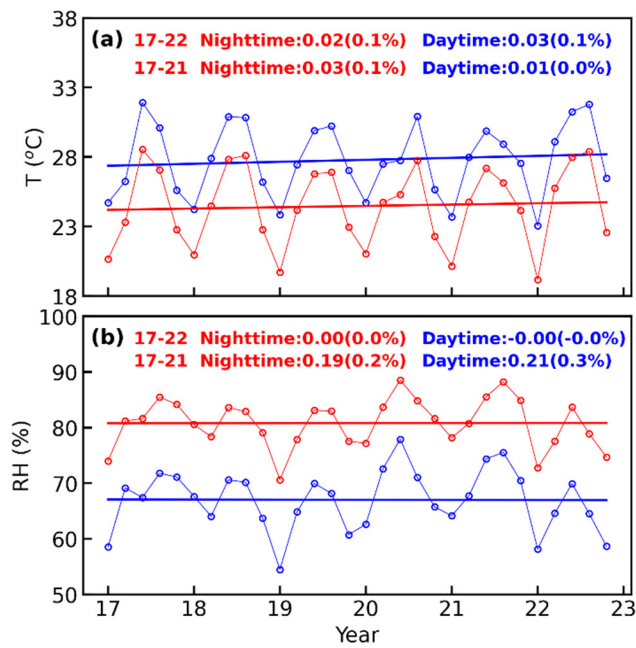

Fig.R3 Trends of observed (a) 98th and (b) 2nd O₃ percentiles (blue lines), meteorological (a) 98th and (b) 2nd O₃ percentiles component (red lines) in MLR simulations, and the anthropogenic (a) 98th and (b) 2nd O₃ percentiles component (magenta lines) in eastern China during May–September 2017–2022. The labels at the top of each panel represent the trend in observed, meteorological, and anthropogenic components.

Table R3. Observed, Meteorologically, and anthropogenically driven trends of 2% and 98% O_3 percentiles in eastern China from 2017 to 2022 and from 2017 to 2021.

| | May–September 2017–2022 trends | | | | | | May–September 2017–2021 trends | | | | | |
| | 2% | | | 98% | | | 2% | | | 98% | | |
	Obs.	Mete.	Anth.	Obs.	Mete.	Anth.	Obs.	Mete.	Anth.	Obs.	Mete.	Anth.
Total	0.115	0.008	0.107	-0.178	0.005	-0.183	0.027	-0.044	0.071	-0.363	-0.119	-0.244
May	0.322	0.017	0.305	-0.020	-0.661	0.641	-0.438	-0.257	-0.181	-3.702	-0.968	-2.734
June	0.205	-0.032	0.237	-4.437	-1.894	-2.543	-0.364	-0.169	-0.195	-2.645	0.124	-2.769
July	0.768	-0.177	0.945	-1.745	-1.100	-0.645	0.665	-0.247	0.912	-2.974	-2.370	-0.604
August	0.371	0.084	0.287	-0.687	-0.156	-0.531	-0.003	-0.260	0.257	-1.473	-0.908	-0.565
September	1.290	0.319	0.971	1.999	1.136	0.863	0.884	-0.126	1.010	1.352	0.814	0.538

Point 4: The authors have not directly answered why the 2nd percentile O_3 increased over 2017–2022. The 2nd percentile should be related to nighttime O_3, while the entire manuscript discusses the O_3 photochemical formation regime, which is a daytime indicator. More investigation is needed on the nighttime process, such as NO titration of O_3, loss of O_3 with VOCs, etc.

Response 4: We agree with this suggestion. Because vertical profiles of O_3 precursors at night are not available due to MAX–DOAS observational limitations, we discuss the possible increase in 2nd O_3 percentile based on surface observations and MLR modelling results. It has been analysed in **Point 3** that the extreme hot and dry in 2022 increases the 98th and 2nd O_3 percentile concentrations, which is mainly a meteorological effect.

If we look carefully at Fig.R2, which presents the anthropogenic impact for each year on the 98th and 2nd percentile trends, respectively, we will find that the observed increase in 2nd O_3 percentile was mainly concentrated after 2020, up to 0.44 ppb/year. The meteorological components did not change significantly in 2020 and 2021 but considerably increased in 2022, with a trend of 0.17 ppb/year 2020–2022. This rapid increase in 2nd O_3 percentile is mainly caused by anthropogenic emissions, with a trend of 0.27 ppb/year 2020–2022. Owing to the impact of the COVID–19 pandemic, the decrease in NO_x concentrations was most significant in 2020–2022 (Fig.3b), and the substantial reduction in NO_x concentrations weakened the O_3 titration of NO, resulting in an increase in nighttime O_3 concentrations, which was also confirmed by the significant negative correlation between the trend of the 98th NO_2 percentile and the trend of the 2nd O_3 percentiles during May–September 2017–2022 (Fig.4b). A recent study showed that nighttime O_3 depletion in China is mainly caused by the wet–scavenging effect and O_3 titration from fresh NO emissions (Li et al., 2023). The wet–scavenging effect

was similar to the effect of precipitation, the higher the ambient humidity, the more conducive it was to O_3 depletion. The RH at night increased slowly in eastern China during May–September of 2017–2021 (Fig.R3b), and the nighttime RH in 2020 and 2021 was higher than that in other years. Moreover, a general wetting trend has been detected in eastern China during the summer in recent years (Hu et al., 2021). RH had the most significant effect on 2nd O_3 percentile trends according to MLR results (Table R1). Therefore, the meteorological component had an inhibitory effect on the increase in the 2nd O_3 percentile trends during May–September 2017–2021. However, owing to the significant emission reduction of NO_x concentrations, the titration of NO_x was weakened, and the decrease in O_3 depletion at night led to an increase in the overall 2nd O_3 percentile trends.

In conclusion, owing to the impact of the COVID–19 pandemic (significant decrease in NO_x concentrations) and unfavorable meteorological conditions (high relative humidity) in 2020 and 2021 in eastern China, the 98th O_3 percentile concentration in 2020 and 2021 was lower (compared to the 98th O_3 percentile concentration in 2018 and 2019), while the 2nd O_3 percentile concentration showed a rapid upward trend. In addition, the extremely hot and dry meteorological conditions in 2022 will increase the 98th and 2nd O_3 percentile concentrations, weakening the decreasing trend in peak O_3 concentrations and increasing the upward trend at low O_3 concentrations. The above discussion was added to the manuscript, please refer to Page 14 Line 31–34 and Page 15 Line 1–18 in the manuscript.
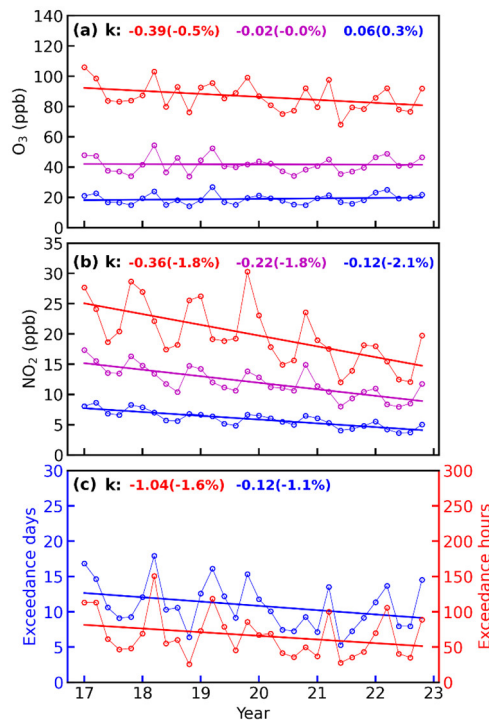
Fig.R4. Trends of surface (a) O_3, (b) NO_2, (c) O_3 exceedance days and O_3 exceedance hours in eastern China during May–September 2017–2022. The red, magenta, and blue solid lines in (a) and (b) indicate the trends for the 98th, 50th, and 2nd percentiles, respectively. The labels on (a) and (b) represent the trends in O_3 and NO_2 for May–September 2017–2022, units: ppb/year. The labels on (c) represent the trends in O_3 exceedance days and O_3 exceedance hours for May–September 2017–2022. The percentage change is indicated in brackets.
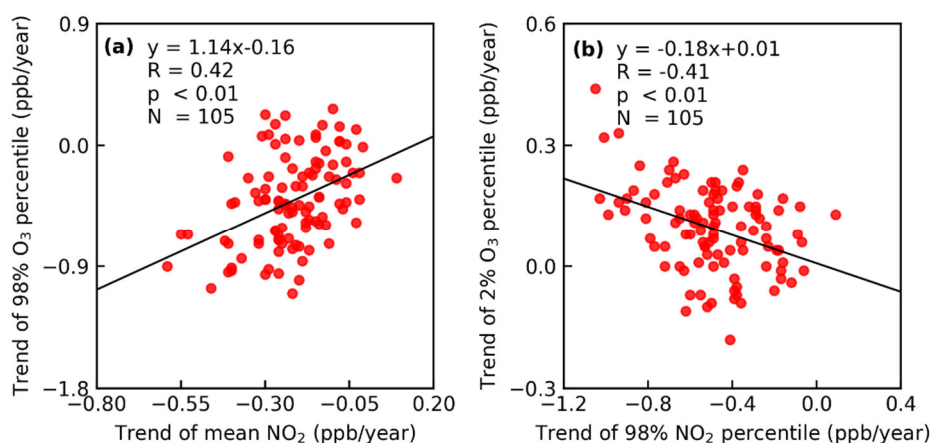
Fig.R5. Scatterplots showing the relationships between the (a) trend of mean NO_2 concentrations and the trend of 98th O_3 percentiles, (b) trend of 98th NO_2 percentiles and trend of 2nd O_3 percentiles in each city of eastern China during May–September 2017–2022. The correlation coefficients are shown in the top left of each panel, N=number of cities.

Point 5: In Section 3.4, although this section should be removed according to my comment #1, conflicts between Figure 9 and Figure S9 are noted. The area proportions presented in Figure 9 are not consistent with the spatial patterns in Figure S9. For example, Figure 9d suggests a NO_x–limited region up to 75% of the total MLYRP in August of 2022, while Figure S9 shows a NO_x–limited area smaller than the VOC–limited area. Please check your analysis.

Response 5: Thanks for pointing out the conflicts among the figures! We carefully examined the reasons for the conflicting images, which were mainly attributed to differences in data processing. Fig.R6 is based on daily FNR to determine the area proportion of the VOC–limited regime, Transition regime, and NO_x–limited regime areas, while Fig.R7 is based on monthly mean FNR to determine the area proportion of the VOC–limited regime, Transition regime, and NO_x–limited regime areas. Fig.R6 shows the trends of TROPOMI observed area proportion for VOC–limited regime, Transition regime, and NO_x–limited regime over Huaihe river basin during May–September 2018–2022. Here we first determined the O_3 formation

sensitivity based on the daily FNR observed by TROPOMI (FNR <2.1 for VOC–limited regime, FNR>3.2 for NO_x–limited regime), and then calculated the area proportion of the daily VOC–limited regime, Transition regime, and NO_x–limited regime areas. Finally, the monthly average of the area proportion of daily VOC–limited regime, Transition regime, and NO_x–limited regime areas was taken and the trend was calculated, as shown in Fig.R6, the light red dots in (b–d) represent the daily values, and the solid red dots are monthly mean values. Fig.R7 shows the spatial and temporal variations of monthly mean FNR from May–September 2018–2022. the monthly mean FNR was calculated firstly based on TROPOMI observed daily FNR, then threshold value 2.1 and 3.2 was used for monthly mean FNR to determine the O_3 formation sensitivity. This section was removed according to **Point 1**.
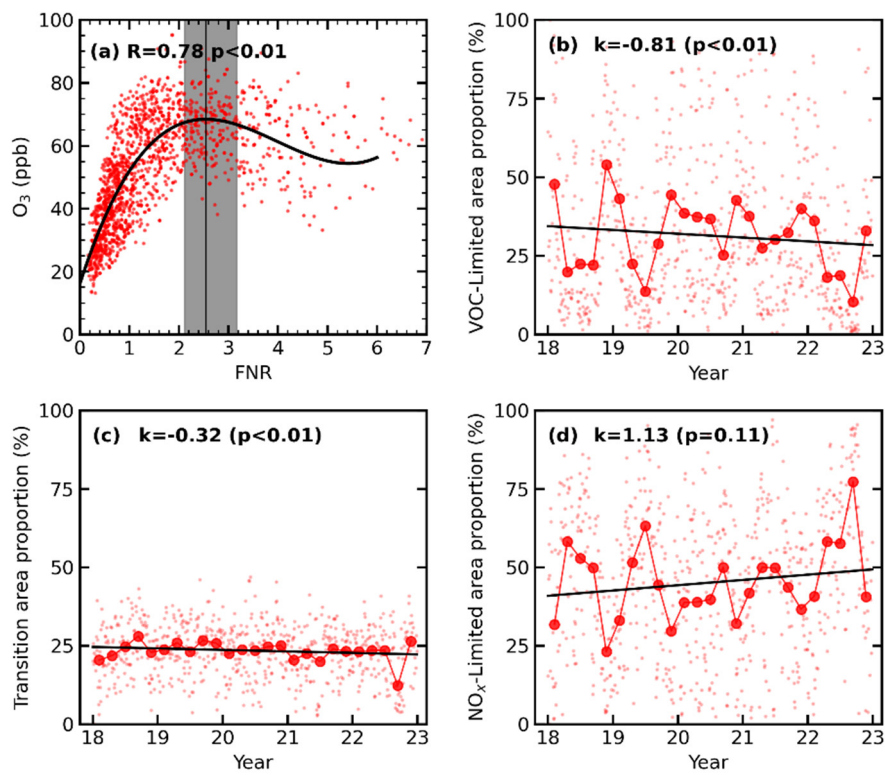
Fig.R6. (a) Variation of monthly mean O_3 (~13:30) with monthly mean TROPOMI FNR in HRB during May–September 2022. The solid line represents third–order polynomial fitting. The vertical line represents the maximum value of the fitted curve, and the vertical shadow represents the range of the curve slope from −3 to +3 (transition regime). Trends of TROPOMI observed area proportion for (b) VOC–limited regime, (c) Transition regime, and (c) NO_x–limited regime over HRB during May–September 2018–2022. The light red dots in (b–d) represent the daily values, and the solid red dots are monthly mean values.
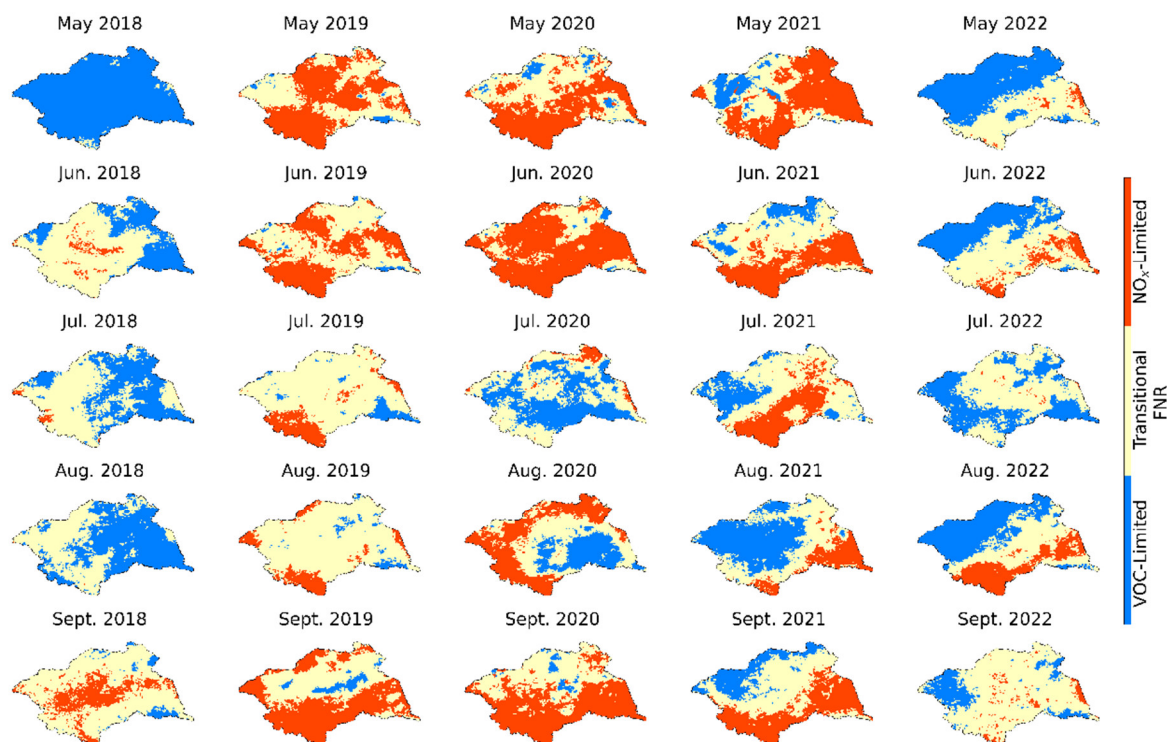
Fig.R7. Spatial and temporal variations of monthly mean FNR from May–September 2018–2022. The date is shown at the top of each panel.

Specific comments:

1. Section 2.3, could the authors elaborate more on how trustworthy is the TROPOMI O$_3$ profile retrieval?

Based on **Point 1,** we have deleted section 3.4 (Interannual differences in surface O$_3$ formation sensitivity), and the O$_3$ profile observed by TROPOMI was not employed in the manuscript. Thus, we also removed the description of the TROPOMI O$_3$ profile retrieval in the manuscript.

2. Lines 20–22, Page 8, could the authors say more about why 5th, 50th, and 95th could represent background, typical, and polluted conditions.

Different percentiles may be related to different influences, such as background concentration levels, emission changes, climate change, and regional transport effects (Lefohn et al., 2010). In principle, the lowest daily O$_3$ concentrations usually occur before sunrise due to nighttime titration of NO, and the low percentile (2nd) usually characterizes baseline or background conditions because increases in the low O$_3$ percentile tend to be associated with increases in baseline or background O$_3$ concentrations. Similar conclusions were also obtained from both models and observations (Jacob et al., 1999; Cynthia Lin et al., 2000). O$_3$ pollution

in eastern China generally occurs in the late afternoon on clear days in the warm season (Wang et al., 2022), when the ambient O_3 concentration is highest, so the high percentile (98th) characterizes the conditions of the pollution events. The middle percentiles (25th, 50th and 75th) usually follow the same trend as the mean values and therefore represent typical conditions (Cooper et al., 2012; Li et al., 2022). We have added this statement to the manuscript, please refer to Page 8 Line 6–17 in the manuscript.

3. Lines 5–6, Page 12: Why is the primary HCHO contribution much higher than the secondary HCHO at these sites, differing from previous findings cited in the paper? Please provide some explanation.

Atmospheric primary HCHO concentrations are mainly derived from motor vehicle exhaust, petrochemical industry, solvent use, and combustion emissions (Ma et al., 2019). Hefei, Huaibei, and Tai'an are located in the NCP, which is the region with the highest primary emissions of air pollutants in China (Li et al., 2017), The rapid industrialization and urbanization in these developing cities has influenced the primary and secondary HCHO concentrations, and HCHO mainly stems from initial atmospheric pollutants (Lu et al., 2024). Although the articles cited in our manuscript show that secondary HCHO concentrations are much higher than that of primary HCHO, the primary HCHO has also been found to be much higher than secondary HCHO in other cities in China, such as Shenyang (Ma et al., 2019), Lanzhou (Lu et al., 2024), Chengdu (Bao et al., 2022), Nanjing (Hong et al., 2018). Primary HCHO concentrations in Hefei, Huaibei and Tai'an usually reach their maximum in the morning and evening, and vehicle emissions may be the main source of primary HCHO, as industrial emissions do not show a significant diurnal pattern (Hong et al., 2018). We have added this statement to the manuscript, please refer to Page 12 Line 9–14 in the manuscript.

Technical corrections:
1. Replace "unbalanced emission reduction in ozone precursors" with NO_x reduction throughout the text?
We have followed this suggestion and carefully checked the manuscript for similar expressions.
2. Line 28, Page 1, remove "experiment".
Thanks for pointing out the unsuitable expression. We have followed this suggestion and corrected the mistake accordingly.
3. Line 25, Page 2, Zhai et al. (2019) is a $PM_{2.5}$ study, not ozone study. Please remove. Also in Line 3, Page 4.

Thanks for pointing out the inappropriate quote, we have corrected the relevant mistakes and carefully checked the manuscript for similar errors.

4. Line 5, Page 3, it should be Li et al. (2020a).

Thanks for pointing out the unsuitable expression, we have corrected the relevant mistakes.

5. Line 22, Page 3, it should be "diagnose".

Thanks for pointing out the unsuitable expression, we have corrected the relevant mistakes.

6. Line 24, Page 8, do not use "one-sided understanding".

We have followed this suggestion and carefully checked the manuscript for similar expressions.

7. In Figure 5, the authors seem to fit the observed monthly O_3 and use the fitted lines to connect monthly values. Please replace these with straight lines directly connecting the dots.

Thanks for your suggestion. We have followed this suggestion and replotted the figure. Please refer to Fig.6 in the manuscript.

8. References, journal names should be included.

Thanks for your suggestion. We have followed this suggestion and reorganized the format of the references.

Reference:

Bao, J., Li, H., Wu, Z., Zhang, X., Zhang, H., Li, Y., Qian, J., Chen, J., and Deng, L.: Atmospheric carbonyls in a heavy ozone pollution episode at a metropolis in Southwest China: Characteristics, health risk assessment, sources analysis, J. Environ. Sci-China, 113, 40-54, 10.1016/j.jes.2021.05.029, 2022.

Cooper, O. R., Gao, R. S., Tarasick, D., Leblanc, T., and Sweeney, C.: Long-term ozone trends at rural ozone monitoring sites across the United States, 1990–2010, J. Geophys. Res-atmos., 117, 10.1029/2012jd018261, 2012.

Cynthia Lin, C. Y., Jacob, D. J., Munger, J. W., and Fiore, A. M.: Increasing background ozone in surface air over the United States, Geophys. Res. Lett., 27, 3465-3468, 2000.

Hong, Q., Liu, C., Chan, K. L., Hu, Q., Xie, Z., Liu, H., Si, F., and Liu, J.: Ship-based MAX-DOAS measurements of tropospheric NO_2, SO_2, and HCHO distribution along the Yangtze River, Atmos. Chem. Phys., 18, 5931-5951, 10.5194/acp-18-5931-2018, 2018.

Hu, W., She, D., Xia, J., He, B., and Hu, C.: Dominant patterns of dryness/wetness variability in the Huang-Huai-Hai River Basin and its relationship with multiscale climate oscillations, Atmos. Res., 247, 105148, 2021.

Jacob, D. J., Logan, J. A., and Murti, P. P.: Effect of rising Asian emissions on surface ozone in the United States, Geophys. Res. Lett., 26, 2175-2178, 1999.

Lefohn, A. S., Hazucha, M. J., Shadwick, D., and Adams, W. C.: An alternative form and level of the human health ozone standard, Inhal. Toxicol., 22, 999-1011, 2010.

Li, K., Jacob, D. J., Liao, H., Shen, L., Zhang, Q., and Bates, K. H.: Anthropogenic drivers of 2013–2017 trends in summer surface ozone in China, Proc. Natl. Acad. Sci., 116, 422-427, 10.1073/pnas.1812168116, 2018.

Li, K., Jacob, D. J., Shen, L., Lu, X., De Smedt, I., and Liao, H.: Increases in surface ozone pollution in China from 2013 to 2019: anthropogenic and meteorological influences, Atmos. Chem. Phys., 20, 11423-11433, 10.5194/acp-20-11423-2020, 2020.

Li, M., Huang, X., Yan, D., Lai, S., Zhang, Z., Zhu, L., Lu, Y., Jiang, X., Wang, N., Wang, T., Song, Y., and Ding, A.: Coping with the concurrent heatwaves and ozone extremes in China under a warming climate, Sci. Bull., 10.1016/j.scib.2024.05.034, 2024.

Li, M., Liu, H., Geng, G., Hong, C., Liu, F., Song, Y., Tong, D., Zheng, B., Cui, H., Man, H., Zhang, Q., and He, K.: Anthropogenic emission inventories in China: a review, Natl. Sci. Rev., 4, 834-866, 10.1093/nsr/nwx150, 2017.

Li, X.-B., Yuan, B., Parrish, D. D., Chen, D., Song, Y., Yang, S., Liu, Z., and Shao, M.: Long-term trend of ozone in southern China reveals future mitigation strategy for air pollution, Atmos. Environ., 269, 10.1016/j.atmosenv.2021.118869, 2022.

Li, X., Ren, J., Huang, R., Chen, L., Li, Y., Qiao, X., Cheng, Y., Zhao, B., Yin, D., Gao, D., Sun, Y., and Zhang, F.: The Aggravation of Summertime Nocturnal Ozone Pollution in China and Its Potential Impact on the Trend of Nitrate Aerosols, Geophys. Res. Lett., 50, 10.1029/2023gl103242, 2023.

Liu, Y., Geng, G., Cheng, J., Liu, Y., Xiao, Q., Liu, L., Shi, Q., Tong, D., He, K., and Zhang, Q.: Drivers of Increasing Ozone during the Two Phases of Clean Air Actions in China 2013–2020, Environ. Sci. Technol., 57, 8954-8964, 10.1021/acs.est.3c00054, 2023.

Lu, C., Li, Q., Xing, C., Hu, Q., Tan, W., Lin, J., Zhang, Z., Tang, Z., Cheng, J., Chen, A., and Liu, C.: Identification of O_3 Sensitivity to Secondary HCHO and NO_2 Measured by MAX-DOAS in Four Cities in China, Remote Sens., 16, 10.3390/rs16040662, 2024.

Ma, Z., Liu, C., Zhang, C., Liu, P., Ye, C., Xue, C., Zhao, D., Sun, J., Du, Y., Chai, F., and Mu, Y.: The levels, sources and reactivity of volatile organic compounds in a typical urban area of Northeast China, J. Environ. Sci-China, 79, 121-134, 10.1016/j.jes.2018.11.015, 2019.

Wang, W., Parrish, D. D., Wang, S., Bao, F., Ni, R., Li, X., Yang, S., Wang, H., Cheng, Y., and Su, H.: Long-term trend of ozone pollution in China during 2014–2020: distinct seasonal and spatial characteristics and ozone sensitivity, Atmos. Chem. Phys., 22, 8935-8949, 10.5194/acp-22-8935-2022, 2022.

Zhai, S., Jacob, D. J., Wang, X., Shen, L., Li, K., Zhang, Y., Gui, K., Zhao, T., and Liao, H.: Fine particulate matter ($PM_{2.5}$) trends in China, 2013–2018: separating contributions from anthropogenic emissions and meteorology, Atmos. Chem. Phys., 19, 11031-11041, 10.5194/acp-19-11031-2019, 2019.

Zhang, T., Deng, Y., Chen, J., Yang, S., and Dai, Y.: An energetics tale of the 2022 mega-heatwave over central-eastern China, Npj Clim. Atmos. Sci., 6, 10.1038/s41612-023-00490-4, 2023.

Zhang, T., Tam, C.-Y., Lau, N.-C., Wang, J., Yang, S., Chen, J., Yu, W., Jiang, X., and Gao, P.: Influences of the boreal winter Arctic Oscillation on the peak-summer compound heat waves over the Yangtze–Huaihe River basin: the North Atlantic capacitor effect, Clim. Dyn., 59, 2331-2343, 10.1007/s00382-022-06212-5, 2022.

Response to Reviewer 2 Comments

Thank you for your decision and constructive comments on my manuscript. We have revised the manuscript carefully according to the reviewers' comments. Point–to–point responses are given below. The original comments are black in color, while our responses are in blue. The revised parts in the manuscript are marked in red. All the page number and line number are referred to the revised manuscript.

Major concerns:

Point 1: How to interpret the variations of low ozone concentrations / background ozone for the targeted region as it's surrounded by polluted areas?

Response 1: In principle, the lowest daily O_3 concentrations usually occur before sunrise due to nighttime titration of NO, and the low percentile (2nd) usually characterizes baseline or background conditions because increases in the low O_3 percentile tend to be associated with increases in baseline or background O_3 concentrations. Similar conclusions were also obtained from both models and observations (Jacob et al., 1999; Cynthia Lin et al., 2000). Li et al. (2014) reported that concentrations below the 5th, between 25th and 75th, and above 95th represent background, typical, and polluted concentrations, respectively. Thus, in our manuscript, low O_3 concentration levels were determined by the 2nd percentiles of hourly O_3 concentrations in each month for cities in eastern China (Li et al., 2022; Cooper et al., 2012; Gaudel et al., 2020). Based on the 2nd O_3 percentile concentrations, we explore the driving forces of the low O_3 trends in eastern China in recent years. Firstly, the Multiple Linear Regression (MLR) model is used to evaluate the anthropogenic and meteorological contributions to the 98th and 2nd O_3 percentile trends. Then, we discuss the impacts of meteorological factors and anthropogenic emissions on low O_3 concentrations, including the impact of the COVID–19 pandemic, and sustained heatwave of extremely hot and dry summer in eastern China in 2022, respectively, and detailed information can be found in the discussion section of the manuscript.

Point 2: How to identify the ozone formation sensitivity based on FNR (ratio of formaldehyde and NO_2).

Response 2: This method belongs to one of the photochemical indicator diagnostics of O_3 formation sensitivity (Chu et al., 2024), and the FNR is the ratio of the volume concentration of HCHO to NO_2. HCHO is a transient product reflecting the oxidation of various VOCs, serving as a proxy for VOCs emissions, as used in previous studies (Zheng et al., 2018; Zhang

et al., 2019). The ratio of NO_2 to NO in NO_x is relatively constant, and the NO_2 concentration can represent the evolution process of atmospheric NO_x. Therefore, HCHO and NO_2 can be taken as representatives of VOCs and NO_x, respectively. This photochemical indicator was originally derived from the photochemical indicator $HCHO/NO_y$ (the ratio of HCHO and NO_y volume concentrations). Jin et al. (2017) suggested that FNR is better suited than $HCHO/NO_y$ for determining O_3 formation sensitivity because both HCHO and NO_2 have short lifetimes (about a few hours), and their ratios can better represent the competition between OH radicals and the reaction between VOCs and NO_2.

This photochemical indicator has been widely used not only in the analysis of ground–based observations, but also in satellite observations, and Martin et al. (2004) were the first to propose the diagnosis of O_3 formation sensitivity based on satellite observations of FNR. Currently, this method has been refined and extended to various O_3 monitoring instrument products (Ren et al., 2022; Chang et al., 2016), such as OMI (Ozone Monitoring Instrument), TROPOMI (Tropospheric Monitoring Instrument) and GEMS (Geostationary Environment Monitoring Spectrometer).

The reliability of surface FNR in the diagnosis of O_3 formation sensitivity was recently assessed by Liu et al. (2021). Based on a joint analysis of multiple in situ observations and model simulations, the validity of FNR in diagnosing O_3 formation sensitivity was determined based on the relative changes in O_3 generation rates with respect to several indicators. Lin et al. (2022) further extended the FNR to the vertical distribution and diagnosed the O_3 formation sensitivity at different altitude using vertical profile of NO_2 and HCHO observed by Multi-Axis Differential Absorption Spectrometer (MAX–DOAS), and the methodology employed in our manuscript is consistent with that of Lin et al (2022).

The advantage of this method is that O_3 formation sensitivities can be quickly determined from photochemical indicators. However, the threshold value of FNR is always the core problem in the application of this method, and its threshold value will change with different environmental conditions, especially the thresholds in different regions tend to differ greatly. Therefore, there are differences in the thresholds reported in different literatures.

Three steps are involved in determining the FNR_{sec} threshold. First, the surface–hourly averaged secondary HCHO and NO_2 VMRs during May–September based on MAX–DOAS observations were normalized by dividing their respective mean values because of the large differences in surface HCHO and NO_2 concentrations (Ren et al., 2022). The ratio of the hourly averaged O_3 VMRs to the hourly averaged normalized NO_2 VMRs (S_{NO2}) and the ratio of the hourly averaged O_3 VMRs to the hourly averaged normalized secondary HCHO VMRs (S_{HCHO})

were calculated. Finally, third–order polynomials were used to fit S_{NO2} and S_{HCHO} (Fig. R1). When S_{NO2} is significantly larger than S_{HCHO}, O_3 formation is more sensitive to NO_x (larger FNR_{sec}), which is the NO_x–limited regime, and vice versa. For example, in Hefei, S_{NO2} and S_{HCHO} intersected at $FNR_{sec}=0.21$. FNR_{sec} less than 0.16 and greater than 0.29 correspond to VOC–limited regime and NO_x–limited regime, respectively, where the relative difference between S_{NO2} and S_{HCHO} is more than 25% (Lin et al., 2022), and the range of FNR_{sec} from 0.16 to 0.29 represents a transition regime.

In addition, following the referee's suggestion, the manuscript was edited by Elsevier Language Editing Services (please see the following Elsevier certificate).
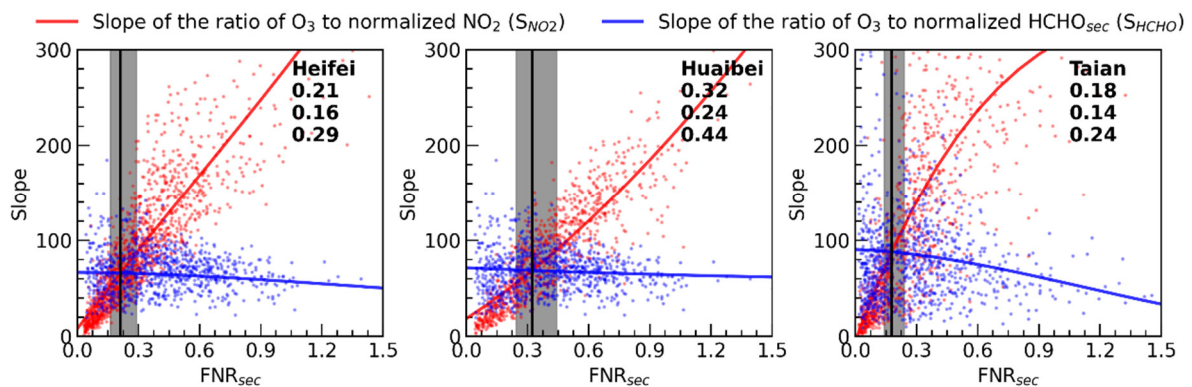

Fig.R1. Three–order fitting of slopes of O_3 VMRs versus normalized NO_2 VMRs and slopes of O_3 VMRs versus normalized secondary HCHO VMRs in different FNR_{sec} values in Hefei, Huaibei, and Tai'an during May–September based on MAX–DOAS observations. The intersect at FNR_{sec} indicated by the black solid line. The vertical shadow indicates the relative difference between the slopes of O_3 VMRs versus normalized NO_2 VMRs and slopes of O_3 VMRs versus secondary HCHO VMRs within 25% (transition regime). The labels at the top right of each panel represent the intersect FNR_{sec} values and the thresholds for the NO_x–limited regime (high) and VOC–limited regime (low) in Hefei, Huaibei, and Tai'an, respectively.

Fig. R2 Certificate of Elsevier language editing services

Detailed comments：

1．Page 1, Line 27: in the main text, you mainly work on "HRB", instead of the whole eastern China. Maybe specifying HRB, instead of eastern China makes more sense.

Thanks for your suggestion. This study attempts to reveal the surface low and peak O_3 trends in eastern Chinese cities in recent years, and to explore the driving forces behind these trends. The surface observations show that the decreased trend in low O_3 concentrations and increased trend in peak O_3 concentrations are widespread in urban agglomerations in eastern China. In the original manuscript, we first analyzed the trend of low and peak O_3 values in the HRB, which were then extended to eastern China. In fact, we conducted MAX–DOAS measurements in three cities in eastern China, namely Hefei, Huaibei and Tai 'an (Fig.R3). First, the three cities are located at similar longitudes with large differences in latitude, transitioning sequentially from south to north. Secondly, the O_3 concentrations of the three cities differed greatly, with Tai' an having a higher surface mean MDA8 O_3 concentration (82.9 ppb), Hefei having a lower surface mean MDA8 O_3 concentration (65.5 ppb), and Huaibei having an intermediate surface mean MDA8 O_3 concentration (74.3 ppb). Therefore, Hefei, Huaibei and Tai 'an can be taken as representative of the 105 cities in eastern China to conduct O_3 precursor observations. In the new manuscript, we have deleted the analysis of the HRB and reorganized the manuscript.

The new manuscript mainly includes four parts. First, we report long–term records of surface O_3 and related parameters observed at urban air quality monitoring sites and by satellites in eastern China, characterizing the trends of low, typical, and peak surface O_3

concentrations during the warm season (May–September) from 2017 to 2022. Then, a Multiple Linear Regression (MLR) model is used to evaluate the anthropogenic and meteorological contributions to the 98th and 2nd O_3 percentile trends. Next, secondary formaldehyde (HCHO) and NO_2 are employed to diagnose the diurnal variations in O_3 formation sensitivity and investigate the reasons for peak O_3 concentration trends in the context of current NO_x reduction. Finally, we discuss the reasons for the potential increase in low O_3 concentrations and the sensitivity of peak and low O_3 trends during the study period. Please refer to our new manuscript for details.
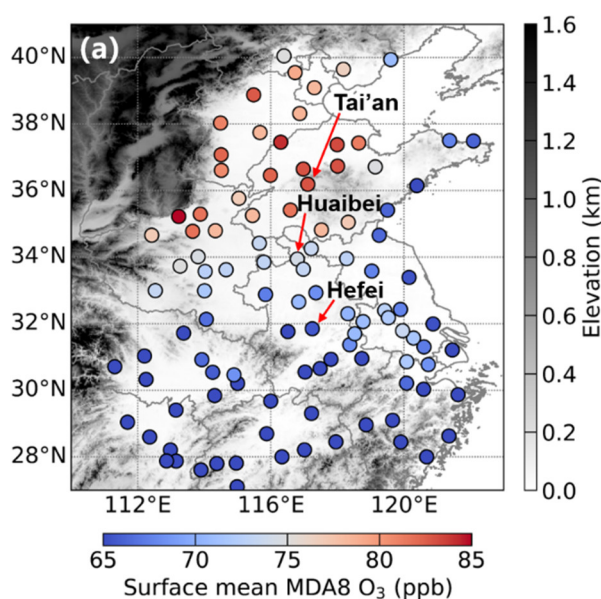

Fig.R3. Spatial distributions of surface mean MDA8 O_3 concentrations during May– September 2017–2022. The red arrow indicates the name of each city, which are equipped with ground–based MAX–DOAS observations

2. Page 1, Line 29: can you elaborate more on the "typical" ozone concentrations?

Thanks for your suggestion. We have followed this suggestion and elaborated more on the "typical" O_3 concentrations. "The decline in typical O_3 concentrations is notably slower than that of peak O_3 concentrations, approximately -0.02 ppb/year (-0.0% per year) during the same period.". Please refer to Page 1 Line 31–32 in the manuscript.

3. Page 1, Line 31: please rephrase the sentence. "Anthropogenic emissions" is not the "cause" of the ozone trends, maybe "driving force" is better.

Thanks for pointing out the unsuitable expression. We have followed this suggestion and corrected it. Please refer to Page 1 Line 33 in the manuscript.

4. Page 2, Line 3: change "on spatial scales" to "spatially".

Thanks for pointing out the unsuitable expression. We have followed this suggestion and removed relevant expressions base on the new abstract.

5. Page 3, Line 5: duplicate reference of Li et al., 2020a

Thanks for pointing out the inappropriate quote, we have corrected it.

6. Page 5, line 18: have you applied consistent AMF (air mass factor) between MAX–DOAS and TROPOMI for NO_2 VCDs?

We did not apply consistent AMF (air mass factor) between MAX–DOAS and TROPOMI for NO_2 VCDs. NO_2 VCDs observed by TROPOMI was downloaded directly from https://search.earthdata.nasa.gov/search (last access: 1 July, 2024). The AMF calculation for MAX–DOAS is a two–step process that first retrieve the atmospheric aerosol vertical profile and then inputs the aerosol vertical profile into the radiative transfer model SCIATRAN, to compute the atmospheric photon paths that are used to convert the NO_2 slanting column concentration into a vertical column concentration (Xing et al., 2017).

7. Page 5, Line 21: why the differences of sensitivity peaks between TROPOMI and MAX-DOAS lead to different HCHO VCD retrievals?

TROPOMI is a space–borne instrument to observe the atmospheric trace gas column concentration from the top down, while MAX–DOAS is a ground–based spectrometer to observe the atmospheric trace gas column concentration from the bottom up. TROPOMI sensitivity peaks in the upper troposphere, which rapidly drops in the atmospheric layers lower than 3 km (Vigouroux et al., 2020), while MAX–DOAS shows an opposite sensitivity that is maximal at the surface and generally becomes negligible above 3 km (De Smedt et al., 2021; Wang et al., 2019). The HCHO concentrations usually concentrated below 2 km over the polluted city (Fig.R4). Therefore, TROPOMI may underestimate the HCHO concentration below 3 km, resulting in a smaller retrieved HCHO VCD. Similar comparative results are also seen in other cities around the world (De Smedt et al., 2021).
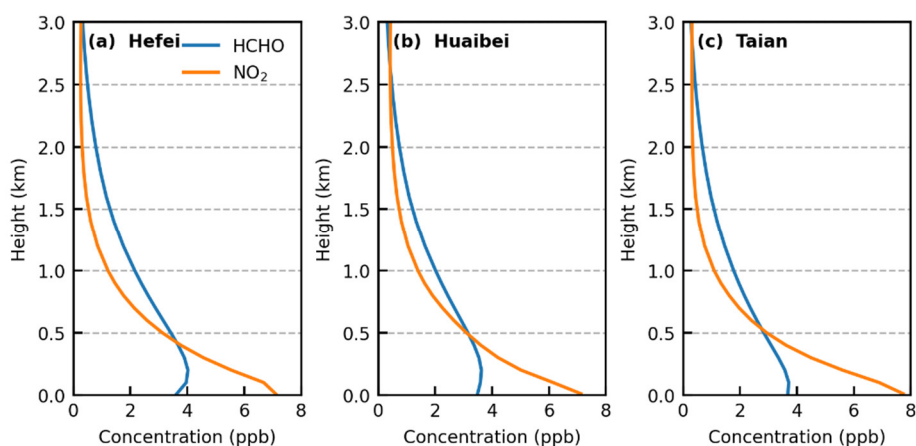
Fig.R4. Mean profiles of NO$_2$ and HCHO concentrations in (a) Hefei, (b) Huaibei, and (c) Tai'an during the whole observation period from May to September.

8. Page 5, Line 24-26: so, what's the conclusion? Are MAX-DOAS data not reliable compared to MEE, as the correlation coefficients are not that high (0.66~0.74)? Please specify it.

The MAX–DOAS data are reliable. Although the correlation coefficients are not that high (0.66~0.74), were also comparable to the comparisons reported in previous studies (Lin et al., 2022; Wang et al., 2020). The differences between MAX–DOAS and MEE observations arise from these two components. First, there was a difference in the detection geometries, as the urban NO$_2$ concentration observed by MAX–DOAS was the result of scanning along a certain direction, whereas the urban NO$_2$ concentration observed by MEE was sampled in situ. Second, there were some differences in their locations, and the urban NO$_2$ concentration of the MEE was the average of several in–situ observation stations (10, 3, and 3 in Hefei, Huaibei, and Tai'an, respectively), whereas we only used one MAX–DOAS in each city. We have added this statement to the manuscript, please refer to Page 5 Line 4–10.

9. Page 6, line 27: this is not true for summer, as VOCs can be dominated by biogenic sources.
Thanks for pointing out the unsuitable expression. We have followed this suggestion and removed relevant expressions.

10. Page 6, Line 28: how about transport from surrounding areas? Especially in HRB, the transport cannot be neglected as it's surrounded by the YRD and Jing-Jin-Ji regions. Please elaborate more.
The effect of transport is included in the meteorological factors, and we considered the effect of horizontal transport (wind speed of u and v components) as well as vertical exchange rates

(vertical velocity at 850 hPa) in MLR fitting. The results also show that horizontal winds and vertical exchange rates are also a key meteorological factor affecting O$_3$ concentrations in many cities in eastern China (Table R1 and R2). The effect of horizontal winds can be seen in two aspects, one is that strong winds blow away high concentrations of O$_3$ and its precursors, and the other is that they bring high concentrations of O$_3$ and its precursors. We also discuss this result in detail in the Discussion section of the manuscript as well. Please refer to Page 14 Line 20–30.

Table R1. Meteorological drivers of 2% O$_3$ percentile and Pearson correlation coefficient between observed and modeled 2% O$_3$ percentile in each city of eastern China during May–September 2017–2022

	Meteorological variable			R		Meteorological variable			R
	1st	2st	3st			1st	2st	3st	
Taian	T	RH	U	0.35	Beijing	U	RH	T	0.23
Puyang	T	BLH	RH	0.50	Tianjing	U	T	RH	0.32
Rizhao	U	V	T	0.46	Baoding	U	RH	TP	0.27
Jining	RH	T	V	0.54	Lanfang	U	T	V	0.23
Xinxiang	U	RH	V	0.41	Shijiazhuang	RH	BLH	U	0.27
Jiaozuo	T	RH	U	0.39	Handan	RH	V	BLH	0.20
Heze	RH	T	V	0.47	Qinghuangdao	V	U	RH	0.32
Linyi	RH	U	TP	0.40	Cangzhou	BLH	T	MSLP	0.28
Kaifeng	RH	U	T	0.49	Xingtai	RH	BLH	U	0.17
Zhengzhou	BLH	RH	U	0.47	Hengshui	T	V	RH	0.28
Luoyang	BLH	RH	V	0.16	Tangshan	U	V	RH	0.20
Zaozhuang	RH	T	U	0.46	Jinan	V	BLH	RH	0.59
Lianyungang	RH	V850	U	0.37	Qingdao	V	BLH	RH	0.26
Shangqiu	RH	T	V	0.48	Zibo	V	BLH	RH	0.59
Xuzhou	RH	BLH	V	0.48	Dongying	U	V	V850	0.36
Xuchang	BLH	RH	U	0.53	Yantai	V	BLH	U	0.33
Suqian	RH	T	MSLP	0.40	Weifang	BLH	T	U	0.34
Huaibei	RH	U	BLH	0.59	Weihai	RH	U	MSLP	0.36
Pingdingshan	BLH	RH	U	0.57	Dezhou	RH	V	BLH	0.40
Bozhou	RH	V	T	0.49	Liaocheng	BLH	V	RH	0.48
Zhoukou	RH	U	T	0.49	Binzhou	BLH	T	V	0.23
Luohe	RH	U	MSLP	0.45	Shaoxing	RH	BLH	T	0.59
Suzhou	RH	U	BLH	0.50	Jinhua	RH	TP	V	0.60
Huaian	RH	V	TP	0.42	Taizhou	V	RH	U	0.54
Yancheng	V	RH	BLH	0.37	Ningbo	RH	V	TP	0.48
Nanyang	RH	U	BLH	0.67	Wuhan	RH	V	BLH	0.61
Zhumadian	RH	TP	BLH	0.52	Changsha	RH	V	BLH	0.71
Fuyang	RH	V	U	0.64	Jinghzou	RH	V	BLH	0.55
Bengbu	RH	BLH	U	0.36	Yueyang	RH	BLH	V	0.60
Huainan	RH	BLH	U	0.56	Zhuzhou	RH	V	BLH	0.73
Xinyang	RH	TP	T	0.63	Xiangtan	RH	V	BLH	0.72
Suizhou	RH	BLH	U	0.63	Yichang	RH	U	V850	0.64
Shanghai	RH	V	TP	0.55	Yiyang	RH	V	BLH	0.67
Nanjing	V	RH	T	0.40	Changde	V	BLH	RH	0.59
Wuxi	RH	V	BLH	0.57	Jingmen	V	RH	U	0.63
Changzhou	V	RH	TP	0.49	Huangshi	RH	U	V850	0.72
Suzhou	RH	V	T	0.52	Huanggang	RH	U	V850	0.77
Nantong	V	RH	U	0.62	Xianning	RH	U	MSLP	0.74

Yangzhou	V	RH	T	0.52	Xiaogan	RH	V850	BLH	0.68
Zhenjiang	V	RH	T	0.55	Quzhou	V	RH	U	0.68
Taizhou	V	RH	T	0.59	Lishui	RH	V	T	0.70
Luan	RH	V	T	0.24	Wenzhou	RH	V	U	0.63
Hangzhou	RH	V	BLH	0.53	Jiujiang	V	RH	MSLP	0.58
Jiaxing	RH	V	T	0.45	Nanchang	V	RH	V850	0.67
Huzhou	V	RH	U	0.61	Jingdezhen	BLH	V850	T	0.59
Hefei	RH	TP	V	0.37	Shangrao	V850	BLH	RH	0.65
Wuhu	V	TP	U	0.46	Yingtan	BLH	V850	RH	0.64
Maanshan	V	U	TP	0.45	Yichun	V850	U	T	0.63
Tonglin	V	T	TP	0.50	Fuzhou	RH	V	BLH	0.72
Anqing	V	T	TP	0.56	Jian	BLH	U	RH	0.57
Chuzhou	RH	V	BLH	0.44	Xinyu	BLH	V	U	0.62
Chizhou	RH	V	BLH	0.47	Pingxiang	V850	BLH	T	0.61
Xuancheng	T	RH	U	0.27	-	-	-	-	-

Table R2. Meteorological drivers of 98% O_3 percentile and Pearson correlation coefficient between observed and modeled 98% O_3 percentile in each city of eastern China during May–September 2017–2022

	Meteorological variable					Meteorological variable			
	1st	2st	3st	R		1st	2st	3st	R
Taian	T	TP	TCC	0.71	Beijing	MSLP	BLH	V	0.30
Puyang	T	V850	TP	0.79	Tianjing	V	MSLP	BLH	0.27
Rizhao	T	U	TCC	0.67	Baoding	MSLP	V	BLH	0.28
Jining	T	TP	V850	0.77	Lanfang	MSLP	BLH	V	0.32
Xinxiang	T	TCC	BLH	0.74	Shijiazhuang	MSLP	BLH	V	0.24
Jiaozuo	T	TP	TCC	0.81	Handan	T	MSLP	U	0.31
Heze	T	V850	TP	0.78	Qinghuangdao	TCC	U	MSLP	0.36
Linyi	T	TP	TCC	0.73	Cangzhou	V	BLH	MSLP	0.35
Kaifeng	T	V850	TP	0.78	Xingtai	MSLP	BLH	V	0.25
Zhengzhou	T	V850	TP	0.78	Hengshui	V	MSLP	BLH	0.38
Luoyang	U	TCC	V	0.28	Tangshan	TCC	MSLP	T	0.27
Zaozhuang	T	TP	TCC	0.81	Jinan	T	TP	V850	0.77
Lianyungang	TCC	U	TP	0.68	Qingdao	U	BLH	RH	0.45
Shangqiu	T	TP	V850	0.71	Zibo	T	TP	V850	0.70
Xuzhou	T	TCC	TP	0.74	Dongying	T	RH	V	0.66
Xuchang	T	V850	TCC	0.70	Yantai	U	T	RH	0.44
Suqian	RH	TCC	TP	0.74	Weifang	T	TP	U	0.68
Huaibei	TCC	T	TP	0.74	Weihai	U	T	RH	0.44
Pingdingshan	T	V850	U	0.66	Dezhou	T	TP	V850	0.75
Bozhou	TCC	T	TP	0.67	Liaocheng	T	V850	TP	0.77
Zhoukou	T	TCC	RH	0.73	Binzhou	T	TP	V	0.66
Luohe	T	V850	RH	0.75	Shaoxing	T	V	TP	0.66
Suzhou	TCC	T	TP	0.71	Jinhua	T	V	TP	0.59
Huaian	T	TCC	TP	0.72	Taizhou	U	V	T	0.62
Yancheng	TP	V850	U	0.56	Ningbo	T	V	U	0.69
Nanyang	T	TCC	RH	0.74	Wuhan	TCC	RH	V850	0.75
Zhumadian	TCC	BLH	TP	0.67	Changsha	RH	TCC	V	0.76
Fuyang	RH	TCC	MSLP	0.74	Jinghzou	RH	V850	T	0.84
Bengbu	T	TCC	TP	0.72	Yueyang	RH	TCC	U	0.82
Huainan	TCC	RH	MSLP	0.68	Zhuzhou	RH	V	T	0.73
Xinyang	RH	TCC	U	0.74	Xiangtan	RH	V	TCC	0.78
Suizhou	RH	TCC	MSLP	0.75	Yichang	RH	TCC	V850	0.79
Shanghai	T	U	RH	0.72	Yiyang	RH	TCC	V850	0.80
Nanjing	TCC	V850	V	0.61	Changde	TCC	V850	T	0.74
Wuxi	TP	TCC	U	0.66	Jingmen	RH	V850	T	0.76

Changzhou	TCC	TP	BLH	0.60	Huangshi	RH	TCC	V	0.76
Suzhou	T	TP	U	0.63	Huanggang	TCC	RH	U	0.72
Nantong	T	RH	BLH	0.75	Xianning	RH	V850	T	0.80
Yangzhou	TCC	TP	V850	0.61	Xiaogan	RH	TCC	U	0.72
Zhenjiang	TCC	TP	MSLP	0.61	Quzhou	RH	V850	T	0.74
Taizhou	TCC	V850	U	0.61	Lishui	RH	U	V	0.65
Luan	TCC	MSLP	T	0.61	Wenzhou	U	RH	V	0.65
Hangzhou	TP	TCC	T	0.69	Jiujiang	TCC	V850	RH	0.80
Jiaxing	T	TP	U	0.70	Nanchang	RH	V850	T	0.72
Huzhou	TP	TCC	T	0.67	Jingdezhen	RH	V850	TCC	0.75
Hefei	TCC	TP	V	0.59	Shangrao	TCC	V850	T	0.76
Wuhu	TCC	TP	V	0.65	Yingtan	TCC	V850	T	0.78
Maanshan	TCC	TP	MSLP	0.66	Yichun	V850	TCC	T	0.75
Tonglin	TCC	MSLP	V	0.63	Fuzhou	V850	T	TCC	0.82
Anqing	TCC	V	TP	0.58	Jian	TCC	T	V	0.66
Chuzhou	TCC	TP	MSLP	0.58	Xinyu	V850	TCC	V	0.75
Chizhou	TCC	V	MSLP	0.63	Pingxiang	V850	TCC	V	0.75
Xuancheng	TCC	V	MSLP	0.58	-	-	-	-	-

11. Page 7, Line 7: so, the perturbations of background ozone are neglected when considering the observed O₃ anomalies. It's not true as transport can contribute to this term.

We thank the reviewer for pointing out this issue. We are also aware of this issue, so we have corrected the MLR model in the manuscript. The updated MLR model first de–seasonalizes the O_3 concentration time series to remove meteorological variability in O_3 concentration. Following Liu et al. (2023) and Li et al. (2020), the MLR model fitted the deseasonalized and detrended 10 d mean 98th or 2nd O_3 percentile time series to the deseasonalized and detrended 10 d mean meteorological variables. The deseasonalized and detrended time series data were constructed by removing the 50 d moving average data from the 10 d moving average data. The stepwise MLR model has the following form:

$$Y(t) = R + \sum_{k=1}^{n} \beta_k X_k(t) \tag{1}$$

Where $Y(t)$ is the deseasonalized and detrended daily surface 98th or 2nd O_3 percentile time series, R is the regression constant, β_k is the regression coefficient, and X_k is the deseasonalized and detrended daily meteorological variable considered as a possible O_3 covariate. Stepwise regressions were performed, adding and removing terms based on their independent statistical significance to obtain the best model fit.

Daily meteorological variables were obtained from the ERA5 reanalysis data (Download from https://cds.climate.copernicus.eu, last access: January 7, 2024), included temperature (T, °C), surface relative humidity (RH, %), total cloud cover (TCC), total precipitation (TP, mm), mean sea level pressure (MSLP, hPa), wind speed of U, V components (U, V, m/s), boundary layer height (BLH, m), and vertical velocity at 850 hPa (V850, m/s).

First, we used the MLR model to remove the effects of meteorological variability from the 2017 to 2022 98th or 2nd O$_3$ percentile trends. We apply Eq. (1) to the meteorological anomalies X_k during May–September 2017–2022, obtained by removing the 6–year means of the 50 d moving averages from the 10 d mean time series. The anomalies calculated in this process were deseasonalized but not detrended. This yields the meteorology–driven 98th or 2nd O$_3$ percentile anomalies $Y_m(t)$

$$Y_m(t) = R + \sum_{k=1}^{n} \beta_k X_k(t) \tag{2}$$

Secondly, to avoid overfitting, only the three most important meteorological parameters were selected based on their individual contributions to the regressed 98th or 2nd O$_3$ percentiles, along with the requirement that they be statistically significant above the 95% confidence level in the MLR model (Li et al., 2018). The fit results and selected meteorological variables varied by city but were regionally consistent (Table R1 and Table R2). The 98th or 2nd O$_3$ percentile anomalies $Y_a(t)$ obtained by deseasonalizing, but not detrending, the 98th or 2nd O$_3$ percentile time series in a similar manner as for the meteorological variables (by removing the 6–year means of the 50 d moving averages). The residual anomaly $Y_r(t)$ after removing the meteorology–driven 98th or 2nd O$_3$ percentile anomalies from the MLR model is given by

$$Y_r(t) = Y_a(t) - Y_m(t) \tag{3}$$

Finally, the residual is an anomalous component that cannot be explained by the MLR meteorological model and is referred to as meteorologically corrected data by (Zhai et al., 2019). It consists of noise due to the limitations of the MLR model and other factors and can be mainly attributed to long–term trends in anthropogenic emission changes over a 6–year period. The trend in the regressed 98th or 2nd O$_3$ percentile reflected the meteorological contribution, and the residual was then used to reflect the presumed anthropogenic contribution. For the updated MLR model, please refer to section 2.4 in the manuscript.

12. Page 8, Line 2: HRB is surrounded by very polluted area, and it can be affected by pollution transport. It's hard to define "background" here, and the background concentrations can change interannually.

We agree with this suggestion, and this is one of the errors in the separation of primary and secondary sources of HCHO by Regression Model. We have extensively reviewed previous studies, and most of the literature has set the background concentration of HCHO at 1 ppb (Sun et al., 2021; Hong et al., 2018; Lin et al., 2022). In addition, according to the ground–level

measurements of HCHO at a rural site in the eastern China by Ma et al. (2016) and Wang et al. (2015), the background level of HCHO near the surface was approximately 1.0 ppb. Therefore, we used this background concentration (1 ppb) in our regression model. Moreover, The fitting results of the regression model are also comparable to those in the previous literature (Hong et al., 2018), so we consider the separation of the primary and secondary sources of HCHO in the manuscript to be reliable.

13. Page 10, line 5: how about the variations in the background?

We have corrected the MLR model in the manuscript (refer to 11). The natural background O_3 concentration is deducted before the stepwise multiple regression. Following Liu et al., (2023) and Li et al. (2020), the natural background O_3 concentration obtained by the 6–year means of the 50 d moving averages from the 10 d mean time series. The new manuscript focuses on the drivers of trends in peak (98th) and low (2nd) O_3 concentrations.

14. Page 10, line 28: do you include nighttime O_3 data in the MLR model? Why?

It is included nighttime O_3 data in the MLR model. This study attempts to reveal the surface low, typical, and peak O_3 trends in eastern Chinese cities in recent years, and to explore the driving forces behind these trends. The 2nd and 98th percentiles of hourly O_3 concentrations in each month for cities in eastern China were calculated to determine their long–term trends at low and peak concentration levels, respectively (Li et al., 2022; Cooper et al., 2012; Gaudel et al., 2020). In principle, the lowest daily O_3 concentrations usually occur before sunrise due to nighttime titration of NO, and the low percentile (2nd) usually characterizes baseline or background conditions because increases in the low O_3 percentile tend to be associated with increases in baseline or background O_3 concentrations.

15. Page 11, Line 2: "(0.108 ppb/year, +114%)", what's this for?

It is the contribution of anthropogenic components on 2nd O_3 percentiles trends. We updated the MLR model in the manuscript, rearranged section 3.2, and removed this description.

16. Page 11, line 27-28: This is weird. When S_{no2} is much larger than S_{hcho} (low FNR), it should be VOC-limited, instead of NOx-limited.

As shown in Fig.R1, the red and blue line represents the S_{NO2} and S_{HCHO}, respectively. When S_{NO2} is much larger than S_{HCHO}, the FNR is higher, and the O_3 formation is more sensitive to NO_x, which is NO_x–limited regime.

17. Figure 6: How do you calculate the slope of the ratio of O_3 to S_{no2}, and the slope of the ratio of O_3 to S_{hcho}? Are you using the ground measurements for all years? Does each point represent the fitted slope each day? I'm curious the temporal intervals between datapoints shown here.

First, the surface–hourly averaged secondary HCHO and NO_2 VMRs during May–September based on MAX–DOAS observations were normalized by dividing their respective mean values because of the large differences in surface HCHO and NO_2 concentrations. The ratio of the hourly averaged O_3 VMRs to the hourly averaged normalized NO_2 VMRs (S_{NO2}) and the ratio of the hourly averaged O_3 VMRs to the hourly averaged normalized secondary HCHO VMRs (S_{HCHO}) were calculated. Finally, third–order polynomials were used to fit S_{NO2} and S_{HCHO} (Fig.R1). S_{HCHO} and S_{NO2} were calculated using data from the warm season (May–September) for all years of MAX–DOAS observations, and each point in Fig.R1 in the manuscript represents the slope for each hour, and the temporal intervals is one hour between datapoints shown in Fig.R1 in the manuscript. We have added this statement to the manuscript, please refer to Page 11 Line 22–27 in the manuscript.

18. Figure 6: I'm curious will the FNR threshold change year by year based on this methodology? How will the interannual variation of the threshold affect your analyses? Please elaborate more.

Differences in the thresholds of the FNR at different times or regions are due to differences in the sources of the corresponding indicator species, whose thresholds vary with environmental conditions (Liu et al., 2021). We calculated the FNR thresholds separately according to different years, and it can be found that the differences in FNR thresholds in different years are very small (FigR5–R7), and the differences in FNR thresholds are mainly between different cities. Therefore, the interannual variation in the threshold have little effect on the results in our manuscript.
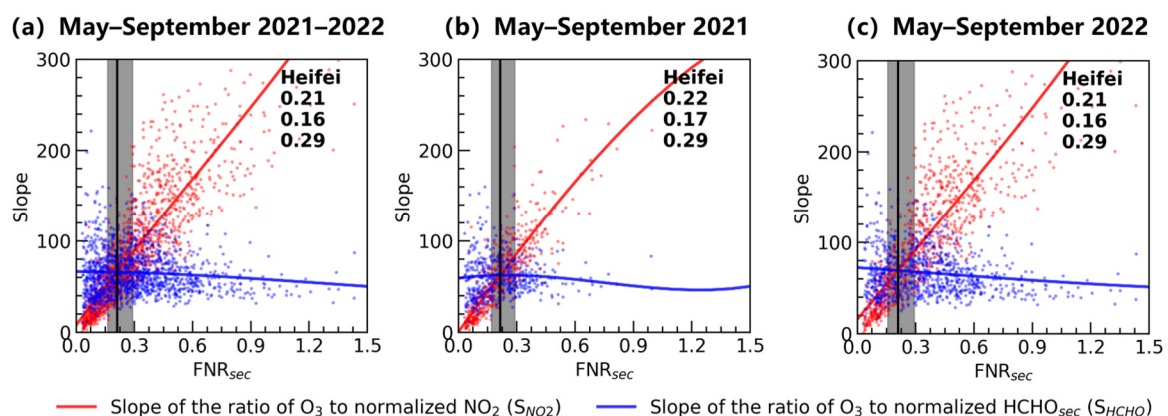

(a) May–September 2021–2022   (b) May–September 2021   (c) May–September 2022

— Slope of the ratio of O_3 to normalized NO_2 (S_{NO2})   — Slope of the ratio of O_3 to normalized $HCHO_{sec}$ (S_{HCHO})

Fig.R5. Three–order fitting of slopes of O_3 VMRs versus normalized NO_2 VMRs and slopes of O_3 VMRs versus normalized secondary HCHO VMRs in different FNR_{sec} values in Hefei, during (a) May–September 2021–2022, (b) May–September 2021, and (c) May–September 2022.
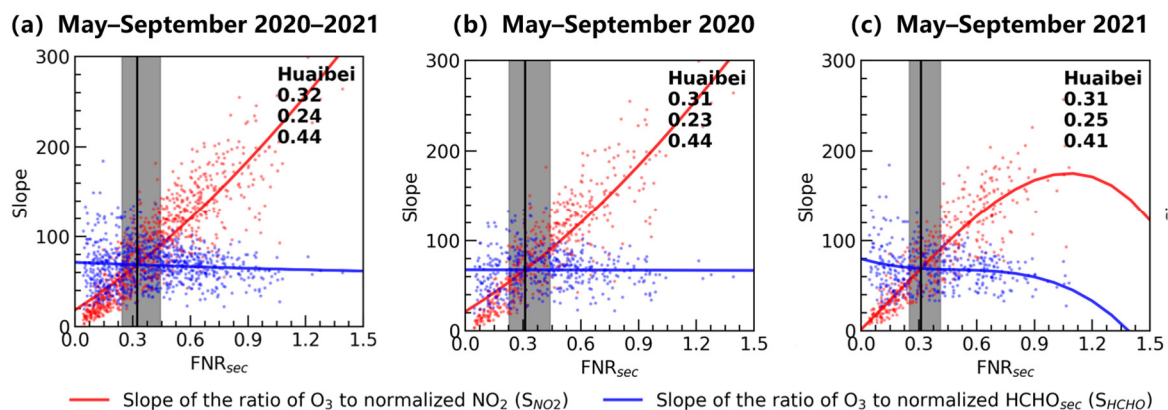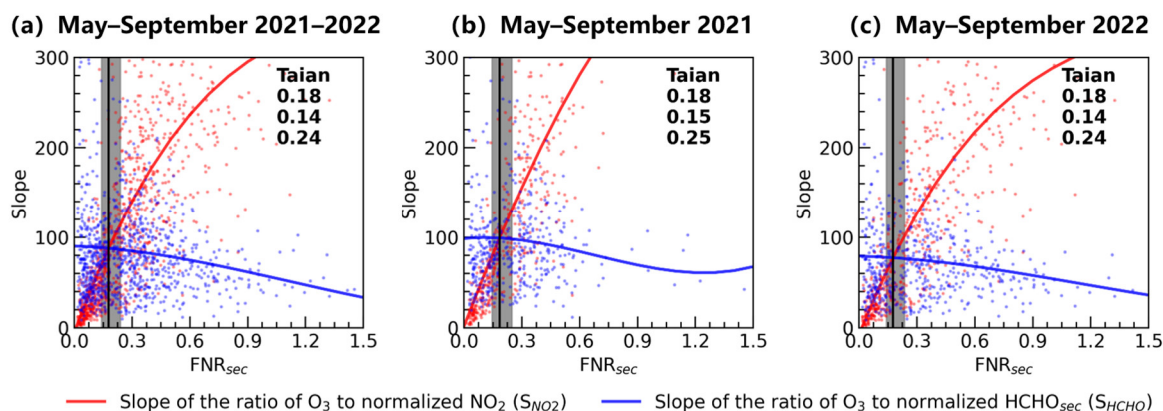

Fig.R6. Three–order fitting of slopes of O_3 VMRs versus normalized NO_2 VMRs and slopes of O_3 VMRs versus normalized secondary HCHO VMRs in different FNR_{sec} values in Huaibei, during (a) May–September 2020–2021, (b) May–September 2020, and (c) May–September 2021.

Fig.R7. The same as Fig.R5 but in Tai'an.

Reference:

Chang, C.-Y., Faust, E., Hou, X., Lee, P., Kim, H. C., Hedquist, B. C., and Liao, K.-J.: Investigating ambient ozone formation regimes in neighboring cities of shale plays in the Northeast United States using photochemical modeling and satellite retrievals, Atmos. Environ., 142, 152-170, 10.1016/j.atmosenv.2016.06.058, 2016.

Chu, W., Li, H., Ji, Y., Zhang, X., Xue, L., Gao, J., and An, C.: Research on ozone formation sensitivity based on observational methods: Development history, methodology, and application and prospects in China, J. Environ. Sci-China, 138, 543-560, 10.1016/j.jes.2023.02.052, 2024.

Cooper, O. R., Gao, R. S., Tarasick, D., Leblanc, T., and Sweeney, C.: Long‐term ozone trends at rural ozone monitoring sites across the United States, 1990–2010, J. Geophys. Res-atmos., 117, 10.1029/2012jd018261, 2012.

Cynthia Lin, C. Y., Jacob, D. J., Munger, J. W., and Fiore, A. M.: Increasing background ozone in surface air over the United States, Geophys. Res. Lett., 27, 3465-3468, 2000.

De Smedt, I., Pinardi, G., Vigouroux, C., Compernolle, S., Bais, A., Benavent, N., Boersma, F., Chan, K.-L., Donner, S., Eichmann, K.-U., Hedelt, P., Hendrick, F., Irie, H., Kumar, V., Lambert, J.-C., Langerock, B., Lerot, C., Liu, C., Loyola, D., Piters, A., Richter, A., Rivera Cárdenas, C., Romahn, F., Ryan, R. G., Sinha, V., Theys, N., Vlietinck, J., Wagner, T., Wang, T., Yu, H., and Van Roozendael, M.: Comparative assessment of TROPOMI and OMI formaldehyde observations and validation against MAX-DOAS network column measurements, Atmos. Chem. Phys., 21, 12561-12593, 10.5194/acp-21-12561-2021, 2021.

Gaudel, A., Cooper, O. R., Chang, K.-L., Bourgeois, I., Ziemke, J. R., Strode, S. A., Oman, L. D., Sellitto, P., Nédélec, P., and Blot, R.: Aircraft observations since the 1990s reveal increases of tropospheric ozone at multiple locations across the Northern Hemisphere, Sci. Adv., 6, eaba8272, 2020.

Hong, Q., Liu, C., Chan, K. L., Hu, Q., Xie, Z., Liu, H., Si, F., and Liu, J.: Ship-based MAX-DOAS measurements of tropospheric NO2, SO2, and HCHO distribution along the Yangtze River, Atmos. Chem. Phys., 18, 5931-5951, 10.5194/acp-18-5931-2018, 2018.

Jacob, D. J., Logan, J. A., and Murti, P. P.: Effect of rising Asian emissions on surface ozone in the United States, Geophys. Res. Lett., 26, 2175-2178, 1999.

Jin, X., Fiore, A. M., Murray, L. T., Valin, L. C., Lamsal, L. N., Duncan, B., Folkert Boersma, K., De Smedt, I., Abad, G. G., Chance, K., and Tonnesen, G. S.: Evaluating a Space-Based Indicator of Surface Ozone-NOx-VOC Sensitivity Over Midlatitude Source Regions and Application to Decadal Trends, J. Geophys. Res-atmos., 122, 10.1002/2017jd026720, 2017.

Li, J., Lu, K., Lv, W., Li, J., Zhong, L., Ou, Y., Chen, D., Huang, X., and Zhang, Y.: Fast increasing of surface ozone concentrations in Pearl River Delta characterized by a regional air quality monitoring network during 2006–2011, J. Environ. Sci-China, 26, 23-36, 10.1016/s1001-0742(13)60377-0, 2014.

Li, K., Jacob, D. J., Liao, H., Shen, L., Zhang, Q., and Bates, K. H.: Anthropogenic drivers of 2013–2017 trends in summer surface ozone in China, Proc. Natl. Acad. Sci., 116, 422-427, 10.1073/pnas.1812168116, 2018.

Li, K., Jacob, D. J., Shen, L., Lu, X., De Smedt, I., and Liao, H.: Increases in surface ozone pollution in China from 2013 to 2019: anthropogenic and meteorological influences, Atmos. Chem. Phys., 20, 11423-11433, 10.5194/acp-20-11423-2020, 2020.

Li, X.-B., Yuan, B., Parrish, D. D., Chen, D., Song, Y., Yang, S., Liu, Z., and Shao, M.: Long-term trend of ozone in southern China reveals future mitigation strategy for air pollution, Atmos. Environ., 269, 10.1016/j.atmosenv.2021.118869, 2022.

Lin, H., Xing, C., Hong, Q., Liu, C., Ji, X., Liu, T., Lin, J., Lu, C., Tan, W., Li, Q., and Liu, H.: Diagnosis of Ozone Formation Sensitivities in Different Height Layers via MAX‐DOAS Observations in Guangzhou, J. Geophys. Res-atmos., 127, 10.1029/2022jd036803, 2022.

Liu, J., Li, X., Tan, Z., Wang, W., Yang, Y., Zhu, Y., Yang, S., Song, M., Chen, S., Wang, H., Lu, K., Zeng, L., and Zhang, Y.: Assessing the Ratios of Formaldehyde and Glyoxal to NO2 as Indicators of O3–NOx–VOC Sensitivity, Environ. Sci. Technol., 55, 10935-10945, 10.1021/acs.est.0c07506, 2021.

Liu, Y., Geng, G., Cheng, J., Liu, Y., Xiao, Q., Liu, L., Shi, Q., Tong, D., He, K., and Zhang, Q.: Drivers of Increasing Ozone during the Two Phases of Clean Air Actions in China 2013–2020, Environ. Sci. Technol., 57, 8954-8964, 10.1021/acs.est.3c00054, 2023.

Ma, Y., Diao, Y., Zhang, B., Wang, W., Ren, X., Yang, D., Wang, M., Shi, X., and Zheng, J.: Detection of formaldehyde emissions from an industrial zone in the Yangtze River Delta region of China using a proton transfer reaction ion-drift chemical ionization mass spectrometer, Atmos. Meas. Tech., 9, 6101-6116, 10.5194/amt-9-6101-2016, 2016.

Martin, R. V., Fiore, A. M., and Van Donkelaar, A.: Space‐based diagnosis of surface ozone sensitivity to anthropogenic emissions, Geophys. Res. Lett., 31, 10.1029/2004gl019416, 2004.

Ren, J., Guo, F., and Xie, S.: Diagnosing ozone–NOx–VOC sensitivity and revealing causes of ozone increases in China based on 2013–2021 satellite retrievals, Atmos. Chem. Phys., 22, 15035-15047, 10.5194/acp-22-15035-2022, 2022.

Sun, Y., Yin, H., Liu, C., Zhang, L., Cheng, Y., Palm, M., Notholt, J., Lu, X., Vigouroux, C., Zheng, B., Wang, W., Jones, N., Shan, C., Qin, M., Tian, Y., Hu, Q., Meng, F., and Liu, J.: Mapping the drivers of formaldehyde

(HCHO) variability from 2015 to 2019 over eastern China: insights from Fourier transform infrared observation and GEOS-Chem model simulation, Atmos. Chem. Phys., 21, 6365-6387, 10.5194/acp-21-6365-2021, 2021.

Vigouroux, C., Langerock, B., Bauer Aquino, C. A., Blumenstock, T., Cheng, Z., De Mazière, M., De Smedt, I., Grutter, M., Hannigan, J. W., Jones, N., Kivi, R., Loyola, D., Lutsch, E., Mahieu, E., Makarova, M., Metzger, J. M., Morino, I., Murata, I., Nagahama, T., Notholt, J., Ortega, I., Palm, M., Pinardi, G., Röhling, A., Smale, D., Stremme, W., Strong, K., Sussmann, R., Té, Y., van Roozendael, M., Wang, P., and Winkler, H.: TROPOMI–Sentinel-5 Precursor formaldehyde validation using an extensive network of ground-based Fourier-transform infrared stations, Atmos. Meas. Tech., 13, 3751-3767, 10.5194/amt-13-3751-2020, 2020.

Wang, M., Chen, W., Shao, M., Lu, S., Zeng, L., and Hu, M.: Investigation of carbonyl compound sources at a rural site in the Yangtze River Delta region of China, J. Environ. Sci-China, 28, 128-136, 10.1016/j.jes.2014.12.001, 2015.

Wang, Y., Dörner, S., Donner, S., Böhnke, S., De Smedt, I., Dickerson, R. R., Dong, Z., He, H., Li, Z., Li, Z., Li, D., Liu, D., Ren, X., Theys, N., Wang, Y., Wang, Y., Wang, Z., Xu, H., Xu, J., and Wagner, T.: Vertical profiles of NO2, SO2, HONO, HCHO, CHOCHO and aerosols derived from MAX-DOAS measurements at a rural site in the central western North China Plain and their relation to emission sources and effects of regional transport, Atmos. Chem. Phys., 19, 5417-5449, 10.5194/acp-19-5417-2019, 2019.

Wang, Z., Liu, C., Xie, Z., Hu, Q., Andreae, M. O., Dong, Y., Zhao, C., Liu, T., Zhu, Y., Liu, H., Xing, C., Tan, W., Ji, X., Lin, J., and Liu, J.: Elevated dust layers inhibit dissipation of heavy anthropogenic surface air pollution, Atmos. Chem. Phys., 20, 14917-14932, 10.5194/acp-20-14917-2020, 2020.

Xing, C., Liu, C., Wang, S., Chan, K. L., Gao, Y., Huang, X., Su, W., Zhang, C., Dong, Y., Fan, G., Zhang, T., Chen, Z., Hu, Q., Su, H., Xie, Z., and Liu, J.: Observations of the vertical distributions of summertime atmospheric pollutants and the corresponding ozone production in Shanghai, China, Atmos. Chem. Phys., 17, 14275-14289, 10.5194/acp-17-14275-2017, 2017.

Zhai, S., Jacob, D. J., Wang, X., Shen, L., Li, K., Zhang, Y., Gui, K., Zhao, T., and Liao, H.: Fine particulate matter (PM2.5) trends in China, 2013–2018: separating contributions from anthropogenic emissions and meteorology, Atmos. Chem. Phys., 19, 11031-11041, 10.5194/acp-19-11031-2019, 2019.

Zhang, Q., Zheng, Y., Tong, D., Shao, M., Wang, S., Zhang, Y., Xu, X., Wang, J., He, H., Liu, W., Ding, Y., Lei, Y., Li, J., Wang, Z., Zhang, X., Wang, Y., Cheng, J., Liu, Y., Shi, Q., Yan, L., Geng, G., Hong, C., Li, M., Liu, F., Zheng, B., Cao, J., Ding, A., Gao, J., Fu, Q., Huo, J., Liu, B., Liu, Z., Yang, F., He, K., and Hao, J.: Drivers of improved PM2.5 air quality in China from 2013 to 2017, Proc. Natl. Acad. Sci., 116, 24463-24469, 10.1073/pnas.1907956116, 2019.

Zheng, B., Tong, D., Li, M., Liu, F., Hong, C., Geng, G., Li, H., Li, X., Peng, L., Qi, J., Yan, L., Zhang, Y., Zhao, H., Zheng, Y., He, K., and Zhang, Q.: Trends in China's anthropogenic emissions since 2010 as the consequence of clean air actions, Atmos. Chem. Phys., 18, 14095-14111, 10.5194/acp-18-14095-2018, 2018.